AIAA AVIATION 2023 Forum

12-16 June 2023, San Diego, CA and Online

# Chemical Kinetics and Thermal Properties of Ablator Pyrolysis Products during Atmospheric Entry

Mitchell R. Gosma<sup>1</sup> and Kelly A. Stephani<sup>4</sup>

Center for Hypersonics and Entry Systems Studies, University of Illinois at Urbana-Champaign, Urbana, IL, 61801

Caleb Harper<sup>2</sup>, Lincoln Collins<sup>3</sup>, and Jeffrey D. Engerer<sup>5</sup> Sandia National Laboratories, Albuquerque, NM, 87123

Legacy and modern-day ablation codes typically assume equilibrium pyrolysis-gas chemistry. Yet, recent experimental data suggest speciation from resin decomposition is far from equilibrium. A thermal and chemical kinetic study was performed on pyrolysis gas advection through a porous char, using the Theoretical Ablative Composite for Open Testing (TACOT). The finite-element tool SIERRA/Aria simulated ablation of TACOT under various conditions. Temperature and phenolic decomposition rates generated from Aria were applied as inputs to a simulated network of continuously-stirred tank reactors (CSTRs) in the chemical solver Cantera. A high-fidelity combustion mechanism computed gas composition and thermal properties of the advecting pyrolyzate. The results indicate pyrolysis gases do not rapidly achieve chemical equilibrium while traveling through the simulated material. Instead, a highly chemically-reactive zone exists in the ablator between 1400-2500 K, wherein the modeled pyrolysis gases transition from a chemically frozen state to chemical equilibrium. These finite-rate results demonstrate a significant departure in computed pyrolysis gas properties from those derived from equilibrium solvers. Under the same conditions, finiterate-derived gas is estimated to provide up to 50% less heat absorption than equilibriumderived gas. This discrepancy suggests non-equilibrium pyrolysis-gas chemistry could substantially impact ablator material response models.

#### Nomenclature

 $\beta$  = Extent of Reaction

 $C_H$  = Stanton number for heat transfer  $C_M$  = Stanton number for mass transfer

 $c_p$  = specific heat (J/(kg\*K)) Da = Damköhler number

 $Da^* = \text{modified Damk\"{o}hler number}$ 

h = mass enthalpy (kJ/kg)

 $\bar{h}$  = bulk virgin carbon-phenolic enthalpy (kJ/kg)

 $\hat{h}$  = normalized enthalpy

k = thermal conductivity (W/(m\*K))

 $m = \max(kg)$ 

 $\dot{m}$  = mass flow rate (kg/s) m'' = mass flux (kg/(m<sup>2</sup>s)) q'' = heat flux (W/cm<sup>2</sup>)  $\dot{q}$  = heat generation (W/cm<sup>3</sup>)

P = Pressure (Pa)

<sup>&</sup>lt;sup>1</sup> PhD Candidate and NSTGRO Fellow, Department of Mechanical Science and Engineering, Member AIAA

<sup>&</sup>lt;sup>2</sup> Undergraduate Researcher, Fire Science and Technology (1532)

<sup>&</sup>lt;sup>3</sup> R&D Scientist and Engineer, Thermal/Fluid Component Sciences (1513)

<sup>&</sup>lt;sup>4</sup> Assistant Professor, Department of Mechanical Science and Engineering, Associate Member AIAA

<sup>&</sup>lt;sup>5</sup> R&D Scientist and Engineer, Fire Science and Technology (1532)

 $\rho$  = density (kg/m<sup>3</sup>)  $\hat{\rho}$  = bulk density (kg/m<sup>3</sup>)

 $\rho_e u_e C'_H$  = convective mass flux (kg/(m<sup>2\*</sup>s))

 $v_m$  = mesh velocity (m/s)

 $\dot{\omega}_q$  = volumetric mass generation from primary pyrolysis (kg/(m<sup>3</sup>\*s))

 $\Delta x$  = length of Aria element (m)  $y_i$  = mass fraction of species i

#### **Subscripts**

c = phenolic char
 e = edge gases
 g = pyrolysis gas
 s = solid ablator
 v = virgin phenolic

# I. Introduction

Low-density carbon-based ablating Thermal Protection System (TPS) materials are an essential component of a variety of atmospheric entry architectures, such as those utilized by SpaceX's Dragon and NASA's Stardust spacecraft. Ablating TPS, such as Phenolic-Impregnated Carbon Ablator (PICA), is typically composed of a carbon-fiber preform and a phenolic-resin matrix. Decomposing thermal protection systems rely on the degradation and pyrolysis of the material to reject the incident thermal load experienced during atmospheric entry. As the phenolic phase degrades, pyrolysis gases are generated in-depth and flow outwards, outgassing into the boundary layer. The residual solid phase constitutes the carbon char, which eventually recedes via oxidation [1,2]. As shown in Fig. 1, distinct regions are formed in the TPS from ablation processes, including fully charred material (char zone), actively pyrolyzing material (pyrolysis zone), and non-degraded material (virgin zone). The gases produced in the pyrolysis zone are critical to thermal management. The outgassing of pyrolysis gases (i.e., 'blowing') isolates the surface from the hot, oxygenrich freestream gases, thereby reducing convective heating, oxidation, and recession at the surface. The gases additionally absorb a substantial amount of heat from the interior of the ablator via the reaction enthalpy of pyrolysis and the advection of thermal energy. Therefore, the accurate characterization of these gas products is critical for the modeling of in-depth ablator material response.

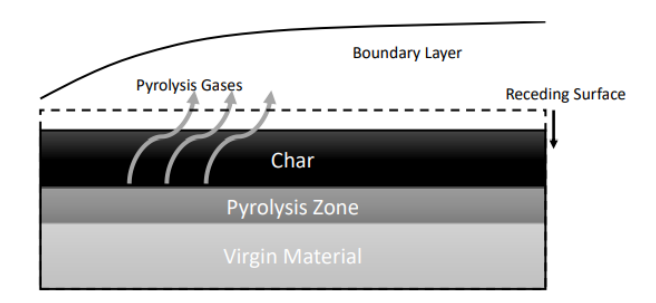


Fig. 1 Ablation of a Carbon-Phenolic TPS during Re-Entry

A variety of ablation codes simulate ablative TPS material response, including Sandia's Charring Materials Ablation (CMA) code and NASA's Fully Implicit Ablation and Thermal response program (FIAT) [3,4]. These legacy codes adopt two major underlying assumptions governing pyrolysis chemistry: 1) Uniform Pyrolysis: The elemental composition of the pyrolysis gases is fixed and 2) Equilibrium Chemistry: Pyrolysis gases always maintain chemical equilibrium. These assumptions substantially simplify pyrolysis-gas characterization and are still widely adopted in modern Type 1 and Type 2 ablation tools [5]. However, the combustion and ablation communities generally recognize these assumptions are not strictly accurate [5,6]. Experimental measurements quantifying elemental and species variations of pyrolysis gases with temperature and reaction extent indicate a departure from equilibrium composition [7-11]. Additionally, the oxygen-deficient and relatively low-temperature environment of the pyrolysis zone may quench chemical kinetics, slowing the progression to chemical equilibrium [12]. While legacy assumptions are easily defensible for the prediction of pyrolysis gas chemistry in regions near-equilibrium (e.g., ablator surface), the resulting gas-property predictions may be inadequate in-depth.

Previous works have attempted to more accurately characterize the composition of in-depth pyrolysis gas. Rabinovitch et al. [12], while primarily interested in investigating equilibrium compositions, used a high-fidelity combustion mechanism [13] to examine the kinetics of pure gas-phase phenol in a highly simplified plug reactor model under a constant velocity and temperature gradient. While the results seemed to verify their hypothesis of heavy formation of polycyclic aromatic hydrocarbons (PAH) at relevant temperatures and residence times, the computed gas mixture was highly dissimilar to the estimated equilibrium composition with initial breakdown of phenol not observed until 1400 K. Lachaud et al. [14] took the step of directly integrating a reduced version of the same combustion mechanism directly into the ablation code PATO. The results of that work again support the hypothesis that pyrolysis gas may be far from equilibrium, however, the testing of the finite-rate model was not a substantial part of the work, and the kinetic pathways of the chemistry model were substantially stripped down to improve computational efficiency.

To effectively analyze the validity of the legacy ablation models, a thermal and chemical study was devised to compare the effects of including non-equilibrium pyrolysis-gas generation and gas-phase chemistry to the equilibrium model. The study was performed using the Theoretical Ablative Composite for Open Testing (TACOT), an open-source ablator material similar to PICA and useful for model comparison [15]. The study was conducted in two phases. In Phase 1, the Sandia National Laboratories thermal/fluids finite element tool SIERRA/Aria [16] performed one-dimensional ablation simulations of TACOT. Aerothermal heating conditions matched those described in the Ablation Test Case Series #2 with the length of the applied heat flux extended to 120 seconds to produce higher temperatures and deeper thermal penetration [15]. Both low- and high-heating cases were performed. In the Aria simulations, the pyrolysis gases are assigned bulk properties from the TACOT source file and the actual composition is neither determined nor tracked. At each discretized timestep of the performed simulations, requisite simulation results were collected for chemical kinetics simulations including temperature, internal gas velocity, pyrolysis-gas generation profiles, extent of phenolic decomposition, and surface recession.

These Aria results are inputs for Phase 2: an examination of the chemical composition and kinetics of the pyrolysis gas. This second phase represents the primary focus of the paper. The open-source Python-based 0D chemistry solver Cantera is employed to model gas chemistry [17]. The 1D environment of Aria is emulated in the Cantera simulation with a network of Continuously-Stirred Tank Reactors (CSTR), where each reactor represents a spatial element from the original Aria simulation. Physical characteristics of the reactors, including mass flow rate, pyrolysis gas generation, residence time, and temperature, are computed based on the Aria simulation results. The chemical kinetics are computed with a robust chemistry mechanism containing most relevant pyrolysis species [13]. This one-way, loosely coupled scheme compares specified Quantities of Interest (QoIs) between the two models subject to either equilibrium or finite-rate chemistry. QoIs include (1) energy generation/absorption of the initial phenol pyrolysis reaction  $(\dot{q}_{decom})$ , (2) advection of thermal energy with the pyrolysis gases  $(\dot{q}_{pgpu})$ , (3) pyrolysis gas chemistry, and (4) pyrolysis gas properties (especially enthalpy). Section II of this paper overviews the thermal and chemical models employed in this study, and Sec. III describes the computational setup in Aria and Cantera. The simulation results are presented and discussed in Sec. IV.

# II. Chemical and Thermal Model

#### A. Ablator Thermal Physics

A key research question in this work is the impact of non-equilibrium pyrolysis-gas chemistry on the overall energy balance of an ablator. A brief overview of the ablator energy balance, as modeled in Aria, is shown in Fig. 2. The overall implementation is similar to CMA and FIAT [3,4]. Starting with the boundary-layer energy balance, the predominant heat source in ablation is the aeroheating of atmospheric gases thermally and chemically excited by a hypersonic shock. Assuming a Lewis Number of unity (equal heat and mass transfer coefficients), the total energy flux from the edge gases incident on the ablator surface is  $\rho_e u_e C'_H h_r$ . The difference between the recovery enthalpy  $h_r$  and the wall enthalpy  $h_w$  yields convective aeroheating heat flux via:

$$q_{aero}^{"} = \rho_e u_e C_H'(h_r - h_w) \tag{1}$$

which is divisible into sensible and chemical heating:

$$q_{aero}^{"} = q_{sens}^{"} + q_{e,chem}^{"} = \rho_e u_e C_H'(h_r - h_{ew}) + \rho_e u_e C_H'(h_{ew} - h_w)$$
(2)

where  $h_{ew}$  is the enthalpy of the edge gases at the wall temperature. The Stanton Number  $C_H$  is generally modified by a blowing correction to account for the effect of surface ablation/pyrolysis gas flux [3]:

$$C'_{H} = C_{H} ln\left(\frac{1+2\lambda B'}{2\lambda B'}\right); \quad B' = \frac{\dot{m}_{S}^{"} + \dot{m}_{g}^{"}}{\rho_{e} u_{e} C_{M}}$$
(3-4)

where B' is a dimensionless mass flow rate and  $\lambda$  is a scaling factor. Now, focusing on the surface energy balance control volume (black region in Fig. 2), the total energy balance of energy conducted into the ablator is expressed as:

$$q_{s,front}^{"} = q_{abs}^{"} - q_{rerad}^{"} + q_{sens}^{"} + q_{e,chem}^{"} + q_{s,chem}^{"} + q_{g,chem}^{"}$$
 (5)

where  $q_{abs}^{"}$  is the absorbed radiation,  $q_{rerad}^{"}$  is re-radiation,  $q_{sens}^{"}$  is the sensible portion of aeroheating, and  $q_{e,chem}^{"}$ ,  $q_{s,chem}^{"}$ , and  $q_{g,chem}^{"}$  represent heat fluxes contributed by chemical reactions of the edge gases (e.g., air), solid ablator gas-surface interactions (i.e., oxidation), and outgassing pyrolyzate, respectively. The last two terms are driven by enthalpy differences between the wall enthalpy and the solid- and gas-phase surface components of the ablator interfacing with the surface (i.e. char and exiting pyrolysis gas) and are defined as:

$$q_{e,chem}^{"} = \dot{m}_{e}^{"}(h_{e} - h_{w}); \quad q_{s,chem}^{"} = \dot{m}_{s}^{"}(h_{s} - h_{w}); \quad q_{g,chem}^{"} = \dot{m}_{g}^{"}(h_{g} - h_{w})$$
 (6)

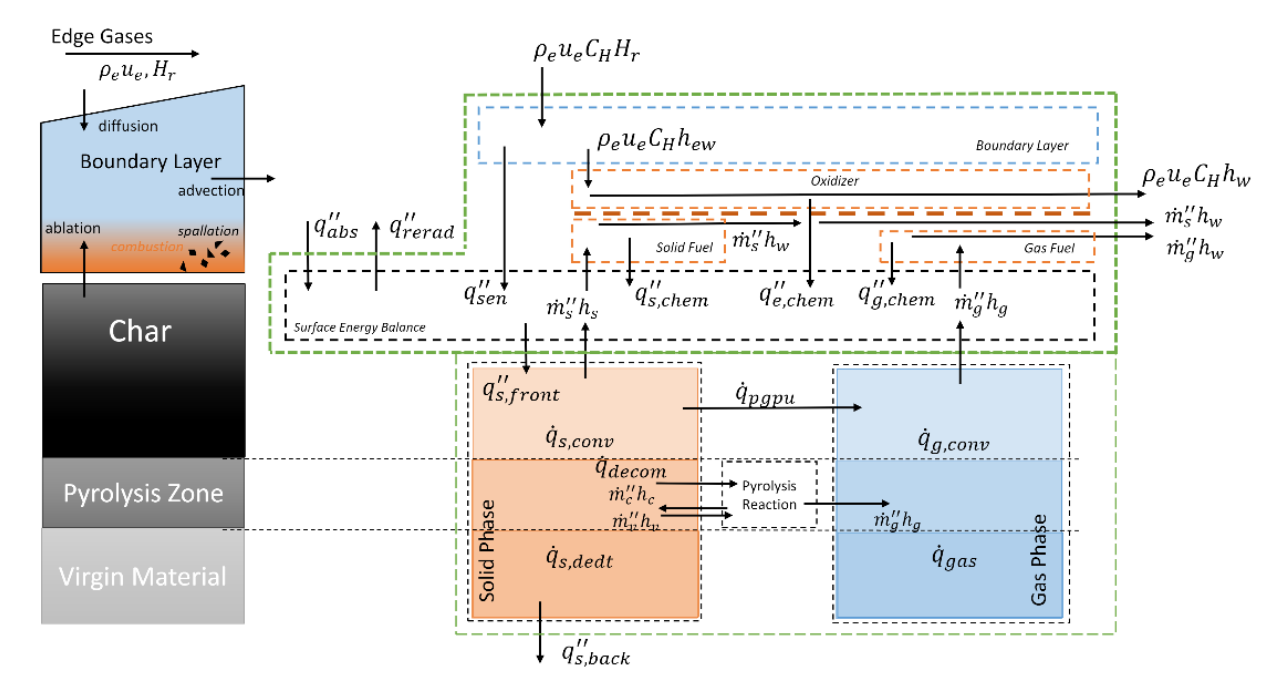


Fig. 2 Energy Balance of an Ablative Material During Re-Entry

Continuing to the physics internal to the ablator, the spatially resolved energy balance for a simulated ablator element is:

$$\dot{q}_{s,sens} + \dot{q}_{cond} + \dot{q}_{s,conv} + \dot{q}_{decom} + \dot{q}_{pqpu} + \dot{q}_{qas} = 0 \tag{7}$$

where  $\dot{q}_{s,sens}$  is sensible heating of the solid,  $\dot{q}_{cond}$  is heat conduction,  $\dot{q}_{s,conv}$  is convection with solids,  $\dot{q}_{decom}$  is decomposition absorption/heating,  $\dot{q}_{pgpu}$  is transpiration driven by sensible and chemical heating, annotated in CMA as pyrolysis-gas pick up [3], and  $\dot{q}_{gas}$  is the change in energy stored by gas in the element. These terms have the following definitions:

$$\dot{q}_{s,sens} = c_{p,s}\hat{\rho}_s \frac{\partial T}{\partial t}; \quad \dot{q}_{cond} = -\frac{\partial}{\partial x} \left( k \frac{\partial T}{\partial x} \right); \quad \dot{q}_{s,conv} = -\frac{\partial}{\partial x} \left( h_s \hat{\rho}_s + c_{p,g} \hat{\rho}_g \right) v_m \tag{8-10}$$

$$\dot{q}_{decom} = (h_{g,\omega} - \bar{h})\dot{\omega}_g; \quad \dot{q}_{pgpu} = -\frac{\partial h_g}{\partial x}\bar{m}_g^{"}$$
 (11-12)

$$\dot{q}_{gas} = c_{p,g} \hat{\rho}_g \frac{\partial T}{\partial t} - \frac{\partial h_g}{\partial x} \tilde{m}_g^{"} - \hat{\rho}_g h_g \frac{\partial h_g}{\partial x} - v_m h_g \frac{\partial \hat{\rho}_g}{\partial x}$$

$$\tag{13}$$

 $\bar{h}$  is defined as:

$$\bar{h} = \frac{\hat{\rho}_V h_v - \hat{\rho}_C h_c}{\hat{\rho}_V - \hat{\rho}_C} \tag{14}$$

This term then encompasses the total enthalpies of the virgin and charred states while correcting for production and consumption rates for each. The values of TACOT are used for the virgin and char ablator enthalpies and bulk densities [13]. The mass flux of pyrolysis gases is partitioned into advection  $(\overline{m}_g^n)$  and correction  $(\overline{m}_g^n)$  terms whereby:

$$\widetilde{m}_g''(x) = \overline{m}_g''(x) + \int_x^L \dot{\omega}_g dx \tag{15}$$

This partitioning of pyrolysis-gas transport ensures the definition of  $\dot{q}_{pgpu}$  is consistent with the legacy definition used by CMA (wherein gas advection is instantaneous) and consolidates second-order terms impacted by gas compressibility [3].

The focus of this study is the two terms in Eq. (7) directly impacted by pyrolysis chemistry: decomposition heating,  $\dot{q}_{decom}$ , and pyrolysis-gas pick up,  $\dot{q}_{pgpu}$ . Their definitions and computation are further elaborated in Sec. IIIB. In short, the pyrolysis gas enthalpy strongly influences the heat absorption from decomposition and transpiration cooling (Eqs. (9-10)). Thus, inaccuracies in gas properties arising from equilibrium assumptions could impact the overall energy balance.

# **B.** Primary Phenolic Pyrolysis

The legacy primary pyrolysis models for carbon-phenolic ablators, including that utilized for the TACOT material, are based largely on the work of Goldstein on CTL-91LD resin [18]. Via thermo-gravimetric analysis (TGA), Goldstein proposed a two-step Arrhenius reaction to model the decomposition of phenolic into carbon char:

$$\frac{dm_t/m_{t,o}}{dt} = \sum_{n=1}^2 -A_n \frac{m_{n,o}}{m_{t,o}} e^{-E_n/RT} \left(\frac{m_n - m_{n,c}}{m_{n,o}}\right)^{\Psi_n}$$
(16)

where  $m_t$  is the overall resin mass,  $m_n$  is the resin mass assigned to the respective reaction n,  $A_n$  is the pre-exponential factor,  $E_n$  is the activation energy, R is the ideal gas constant, T is temperature, and the subscripts o and c refer to initial (i.e., virgin) and final (i.e., char) values, respectively. The fitted Arrhenius parameters determined by Goldstein for Eq. (16) are listed in Table 1. The phenolic mass is partitioned into two parallel reactions. The char yield of 50% is assigned to the second reaction. More complex mechanisms have been proposed in the literature based on modern experimental data [19,20], but the TACOT decomposition model was sufficient for the objectives of the present study.

Table 1. Pyrolysis Reaction Mechanism [18]

Reaction	A, s <sup>-1</sup>	<i>E/R</i> , K	Ψ	$\frac{m_{n,o}}{m_{t,o}}$	$\frac{m_{n,c}}{m_{t,o}}$
1	$1.40 \times 10^4$	8560	3	0.25	0.0
2	$4.48 \times 10^9$	20450	3	0.75	0.5

As previously mentioned, most legacy ablation models assume the uniform production of pyrolysis gases, wherein the elemental composition is constant with respect to temperature and reaction extent. This definition is true for TACOT, which recommends a pyrolysis elemental mole fraction of 20.6 % Carbon, 67.9% Hydrogen, and 11.5% Oxygen, based on the work of Sykes [11]. Leveraging this fixed mass fraction and assuming a gas composition in chemical equilibrium, the pyrolysis gas property table for TACOT was generated using CEA [12].

Experimental measurements of pyrolysis-gas composition demonstrate elemental and species vary with temperature and reaction extent [7-11]. In 2017, Bessire and Minton produced an in-depth study of volatile pyrolysis gas products produced by PICA subjected to various heating rates [10]. In their work, samples of virgin PICA ablator were heated in a vacuum environment at various rates, with outgassed primary pyrolysis species measured using a mass spectrometer. For each heating rate, the authors produced detailed measurements of specimen mass loss (via TGA) and molar production rates of primary pyrolysis species as a function of temperature. Consistent with previous literature [19], the data from the  $6.1^{\circ}$ C s<sup>-1</sup> ramp rate determines the pyrolysis gas mixture used in our analysis. Instead of temperature, we choose to characterize the composition in terms of reaction extent  $\beta$ :

$$\beta = \frac{\hat{\rho}_V - \hat{\rho}}{\hat{\rho}_V - \hat{\rho}_C} \tag{17}$$

The proposed speciation model, dependent solely on reaction extent, strips temperature dependence from the original dataset. This derivation is useful because the validity of the experimental temperature measurements has been questioned [21], and should allow for the recreation of the overall production-averaged gas composition despite using the legacy Goldstein decomposition model.

Based on the Bessire speciation data, and assuming that the final recorded mass represents a fully charred sample ( $\beta=1$ ), we compute  $\beta$  as a function of temperature and then examine the elemental mole fractions of the produced pyrolysis gas as a function of reaction extent. The results for the 6.1 °C s<sup>-1</sup> case are shown in Fig. 3. Elemental composition varies significantly with reaction extent. Water is by far the most common pyrolysis product during the initial stages, followed by CO and CO<sub>2</sub>. As the reaction progresses, the contribution of oxygen declines as methane and other hydrocarbons begin to contribute significantly. At later reaction extents, diatomic hydrogen begins to dominate, reducing the relative elemental contributions of carbon and oxygen. The observed "spikes" in the data at around  $\beta=0.05$  is due to an initial significant measurement of propenal observed by Bessire and Minton at low temperatures. Integration of the molar production curves found in the supplementary data of Bessire and Minton [10] yields an average elemental composition of 18.0 % Carbon, 66.2 % Hydrogen, and 15.8 % Oxygen by mole fraction.

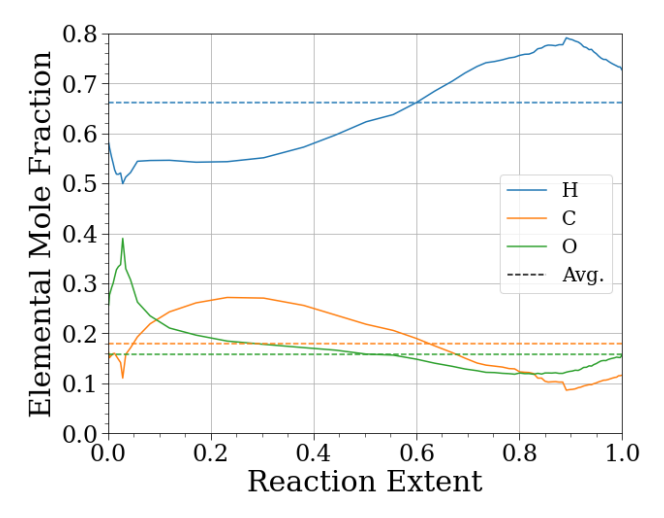


Fig. 3 Experimental Elemental Mole Fractions of PICA Pyrolysis Gas, 6.1 °C s<sup>-1</sup> Heating Rate [10]

Not all the primary pyrolysis gas species in the Bessire-Minton data are included in the used gas-phase chemistry mechanism, which will be discussed in the following section. As a result, several of the gas products are substituted for more common species, as outlined in Table 2. These substitutions are intended to preserve the elemental and mass balances but may neglect some important chemical effects. If high-fidelity ablator chemistry is pursued in the future, these approximations should be reevaluated. Applying these substitutions, the species composition of the modeled primary pyrolysis gas is shown in Fig. 4.

While the data presented in Figs. 3-4 demonstrates the non-uniform nature of primary pyrolysis, the data does not necessarily undermine the legacy model assumption of chemical equilibrium. Non-equilibrium species could rapidly reach equilibrium, rendering their initial existence trivial. Pyrolysis across the range of temperatures and reaction extents within the pyrolysis zone could result in reasonably uniform pyrolysis gas chemistry. Further modeling of the

chemical kinetics is required to demonstrate that further study is warranted, leveraging these experimental results, as presented here.

**Table 2. Molar Substitutions for Missing Species** 

Species	Substitution		
1-Propanol	Propenal + 2H <sub>2</sub>		
2-Propanol	Propenal $+ 2H_2$		
Xylene	Toluene $+ CH_4 - H_2$		
Dimethyl Phenol	Phenol $+ 2CH_4 - 1.5H_2$		
Trimethyl Phenol	$Phenol + 3CH_4 - 2.5H_2$		

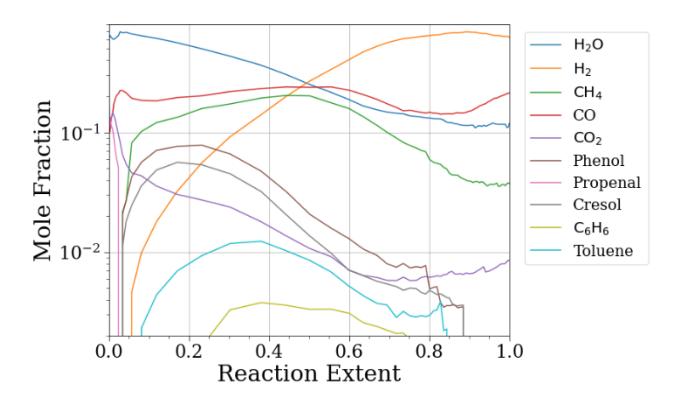


Fig. 4 Species Composition of Modeled Primary Pyrolysis Gas

# C. Secondary Pyrolysis

After initial decomposition, the pyrolysis products advect through the char towards the boundary layer. The gas mixture can exist in three different chemical states, depending on conditions: (1) the mixture remains chemically inactive (i.e., frozen), (2) quickly achieve chemical equilibrium, or (3) experiences an extended period of non-equilibrium finite-rate chemistry. In most legacy ablation codes, the rapid equilibrium assumption is utilized. As was done with TACOT, equilibrium chemistry solvers intake the elemental fractions and compute the corresponding chemical state under specified temperature and pressure conditions [5]. Historically, this approach was an assumption of necessity – finite-rate chemistry models were predominantly unavailable, and computational capabilities were severely limited.

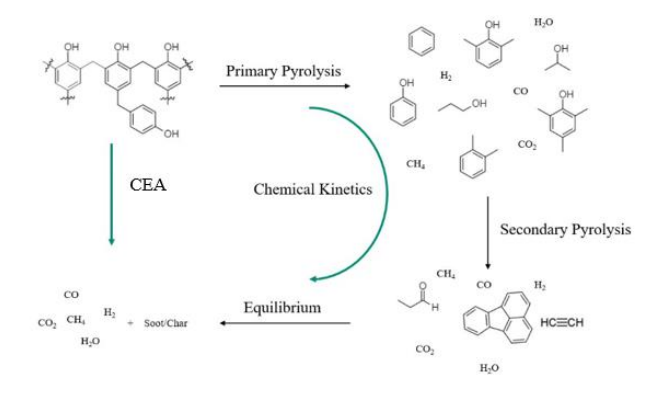


Fig. 5 Pyrolysis Chemistry Pathways

Figure 5 shows the simulated and actual pathways for pyrolysis gas chemical kinetics. The original phenolic resin decomposes into primary-pyrolysis products. The formed gases then experience additional heating and undergo chemical reactions, eventually reaching an equilibrium state. The time required to attain chemical equilibrium varies widely depending on environmental conditions in the ablator, especially temperature. Substantial differences in gas

species composition likely exist between a finite-rate and equilibrium model within the ablator, resulting in differing gas enthalpies – thus impacting thermal response. Therefore, we seek to identify the validity of the equilibrium assumption and additionally determine quantitatively the difference in thermal transport between finite-rate and equilibrated gas mixtures (both TACOT and that produced from Bessire and Minton data [10]) via decomposition and pyrolysis gas pick-up enthalpy terms.

The chemical state is ultimately determined via both homogeneous and heterogeneous chemical kinetics. Heterogeneous kinetics refers to potential reactions between the pyrolysis gas and the solid carbon-fiber matrix of the ablator. Relevant to this study is the possibility of carbon deposition reactions (e.g. coking) in the char layer [12,14]. For simplicity, heterogeneous reactions are ignored in this study due to the conditions modeled. Based on the work on Lachaud [22], if a PICA pore-diameter of 50 µm (aka the characteristic length) and an average pyrolysis gas molecular diameter like that of oxygen in air is assumed, then at atmospheric pressure the local Knudsen number of modeled internal flow is less than 0.02 for temperatures below 3000 K. This indicates that the pyrolysis gas is in the continuum regime, and chemistry should be largely dominated by homogenous reactions. However, the neglecting of heterogeneous chemistry may ignore important chemical source/sink terms, potentially necessitating future examination.

The chemistry model utilized in this study for homogeneous gas-phase reactions is a high-temperature hydrocarbon combustion mechanism originally developed in the work of Blanquart et al. [13]. The most recently released version of CaltechMech contains a total of 172 species and 1896 reactions (counting forward and reverse reactions separately). The model contains most of the primary pyrolysis species from Bessire and Minton [10], and critically contains all major formation pathways for PAHs. PAHs are an important potential speciation product of hydrocarbon combustion and are theorized to constitute a critical precursor to soot formation or coke formation during combustion processes [12,23]. Solid-phase carbon species are often considered to be a major component of equilibrated pyrolysis gas [24], however, the full kinetics of this  $PAH \rightarrow soot/coke$  pathway is complex and underexplored. For the purposes of this study, we will neglect the possibility of soot formation or PAH-fiber deposition and proceed with modeling the finite-rate chemistry and computed equilibrium states using only species in the Blanquart mechanism.

# **III. Simulation Set-up**

#### A. TACOT Simulations in Aria

As mentioned, ablation and pyrolysis results were generated using SIERRA/Aria, a generalized thermal/fluids modeling finite-element code developed by Sandia National Laboratories (SNL) [16]. Aria is a Galerkin finite element-based program built to solve PDE-driven coupled-physics problems. Support exists for nonlinear, transient, implicit, and direct to steady-state problems in both 2D and 3D, bolstered by a suite of physical models including species and thermal energy transport. The Arbitrary Lagrangian-Eulerian (ALE) formulation for mesh generation improves efficacy for modeling fluid-structure interaction and multi-phase materials. A code verification study of Aria as an ablation tool was recently published in the work of Freno et al. [25], and the recent work of Collins and Roberts demonstrates the applicability in the design process and optimization of woven TPS composites via mesoscale simulations [26].

The Aria implementation deployed herein included the physics implementation of CMA with the additional capability of modeling porous-media flow via a Darcy-flow solver. This implementation is consistent with a Type 2 ablation code under the classification of Lachaud [5]. The thermal physics and energy balance resolved in the finite element model is described in Section IIA. The predicted char removal rate and pyrolysis gas mass flow rate at the surface compute the recession rate and wall enthalpy via TACOT B' tables [14]. Recession is then enforced as a surface displacement using a mesh-deformation model. The transport equations include advective corrections that account for the ALE approach applied here (e.g. Eq. (13)). The deployed model does not track individual pyrolysis gas species or contain a finite rate chemistry model for gas-phase reactions. Instead, the standard tabulated pyrolysis gas properties of TACOT are used in Aria. Solid-phase ablator properties (e.g., conductivity, porosity) are interpolated from tabulated TACOT virgin and char properties based on reaction extent  $(\beta)$ .

The modeled ablation simulations follow the  $2^{nd}$  Ablation Test Case Series developed by Lachaud et al. at the University of Kentucky [15]. A one-dimensional sample of TACOT, 5.0 cm in length with an initial temperature of 300 K, is heated at atmospheric pressure with an aerothermal heating condition and an adiabatic boundary condition on the inward-facing surface. The porous space within the ablator is initially filled with pyrolysis gases at 300K. Two modified versions of the simulations described by Lachaud (Cases 2.2-2.3) were performed. The critical parameters for each test case are listed in Table 3, described herein as Cases 1 (high-heating rate) and 2 (low-heating rate). Reradiation effects are modeled under a prescribed far-field temperature,  $T_{\infty}$ , of 300 K with supplied emissivity values, and the legacy blowing correction model of CMA is applied with  $\lambda$  set to 0.5 [3].

The original TACOT cases include 60 seconds of heating followed by a 60-second cooldown [15]. These conditions were modified herein. The applied heating was extended to 120 seconds to enable better examination of in-depth material response and produce a larger temperature gradient of gas-phase results to examine in Cantera. The cooling phase is omitted for each simulation, leaving a total simulation time of 120.1 seconds. A fixed timestep scheme was used with a temporal resolution of 0.05 s. The TACOT ablator was resolved as a quasi-1D stack of 100 hexahedral finite elements. At each timestep, gas-phase temperature, velocity, pyrolysis gas generation, and mesh displacement due to recession were post-processed for use in the subsequent Cantera study. Atmospheric pressure was assumed on the ablator surface. Due to the high permeability of TACOT, pressure gradients were minimal and are neglected in the Cantera simulation.

**Table 3: Environment Properties for Aria Test Cases** 

Case	Time, s	$T_{\infty}, K$	Tsurf, K	$h_r \rho_e u_e C_H$ , $Wm^{-2}$
1	120.1	300	3200	$7.5 \times 10^6$
2	120.1	300	1600	$4.5 \times 10^{5}$

#### **B.** Cantera Models

Cantera is an open-source code designed to compute chemical kinetics and resulting thermodynamic states [17]. Native capabilities include a variety of zero-dimensional reactors which can be linked to form reactor networks. Relevant applications include one-dimensional flames, adiabatic chemistry, equilibrium calculations, the calculation of thermodynamic quantities (e.g., enthalpy), and various chemical-kinetics models. The work herein leverages Cantera's 0D reactor models and networks thereof, alongside a chemical kinetics database for pyrolysis and combustion.

Figure 6 shows the primary reactor type utilized in this study. A Continuously-Stirred Tank Reactor (CSTR) is a uniformly mixed reservoir of reacting fluid that includes both inlet and outlet flow. Species are 'well-mixed', thus enforcing uniform temperature and concentrations throughout the full volume. Species react over time, often under isothermal or adiabatic conditions. Species enter the reactor from inlet reservoirs with specified conditions and gas composition. Species have a finite residence time in the CSTR and can exit the reactor before reaching equilibrium.

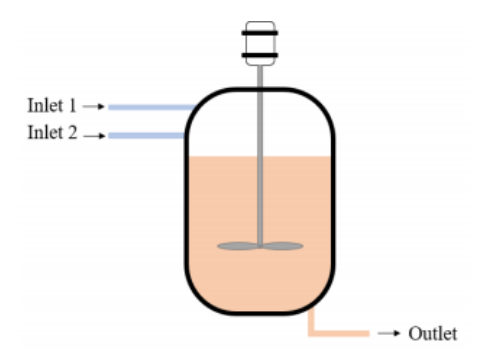


Fig. 6 Simplified Diagram of a CSTR

For isothermal, constant-pressure reactors in Cantera, the species mass balance is considered. The CSTR is at a steady-state mass-flow condition, so the overall mass balance is trivial ( $\dot{m}_{in} = \dot{m}_{out}$ ). Accounting for species generation, consumption, accumulation, and mass flow rate, the change of mass fraction of a species i with respect to time is [17]:

$$m\frac{\partial y_i}{\partial t} = \sum_{in} \dot{m}_{in}(y_{i,in} - y_i) + \dot{m}_{i,chem}$$
(18)

where  $\dot{m}_{in}$  constitutes gas entering the reactor through any number of inlets, and  $\dot{m}_{i,chem}$  represents the creation/destruction of species i due to in situ chemical reactions.

The chemistry of an ablator features a porous medium, spatially distributed inlets (i.e., pyrolysis), a temperature gradient, and a single outlet (external surface). This porous chemistry geometry is effectively a Packed-Bed Reactor (PBR), with fluid flow and homogeneous reactions within the open-porous structure, and heterogeneous reactions (i.e., packed bed) at the pore walls (i.e., fibers, and resin char). The upper part of Fig. 7 visualizes this PBR model;

pyrolysis gas generation (represented as  $I_n$ ), mass flow, and temperature profiles are continuous. While this representation is physically accurate, Cantera reactor models do not directly support one-dimensional, multi-inlet, plug-flow reactors. Instead, Cantera approximates these systems using zero-dimensional reactor networks. Here, we approximate the PBR reactor with a series of discretized CSTRs as shown in the lower section of Fig. 7. Boundary conditions applied to this multi-inlet CSTR network model include temperature, pyrolysis rates, and gas velocity profiles.

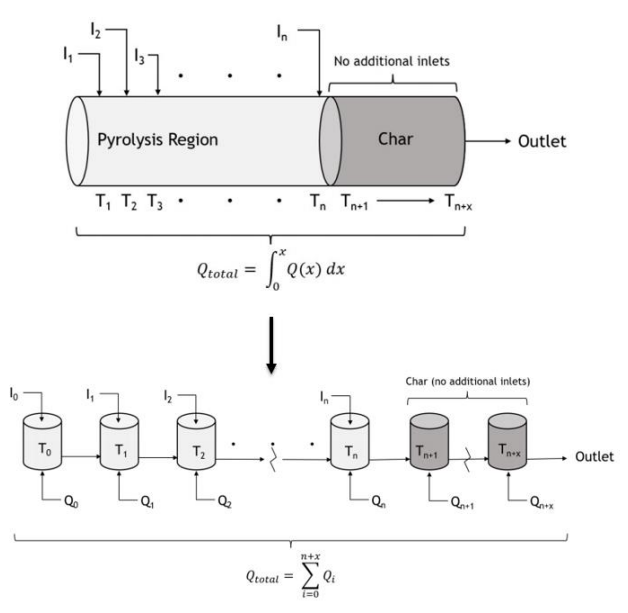


Fig. 7 Diagram of an Idealized Packed-Bed Reactor to Represent Pyrolysis Gases in a Charring Ablator (Top), and the 0-D CSTR Reactor Approximation Created in Cantera (Bottom)

Under this model, each reactor has two inlets, one for generated primary pyrolysis gases and one for flow from the previous reactor. Accounting for these inlets and outlets and normalizing by volume, Eq. (18) can be rewritten as:

$$\hat{\rho}_g \frac{\partial y_i}{\partial t} = \frac{(y_{i,in} - y_i)}{\Delta x} m_{g,in}^" + (y_{i,\omega} - y_i) \dot{\omega}_g + \dot{\omega}_{i,chem}$$
(19)

where  $\dot{m}_{in}$  has been segregated into contributions from the previous reactor  $(m_{g,in}^{"})$  and those from primary pyrolysis  $(\dot{\omega}_g)$ .

The Cantera simulations consider only the homogeneous reactions and gas advection. Temperatures, pyrolysis rates, reaction extent  $\beta$ , and velocities are obtained from Aria simulations of TACOT [12]. Pore-space expansion and gas molecular-weight and compressibility effects are neglected from the overall reactor network flow rate. Each Cantera reactor corresponds to an element in Aria (100 elements/reactors). This approximation of the gas-flow state matches the definition of the pyrolysis gas pick-up in Eq. (12) and neglects the additional terms in  $\dot{q}_{gas}$  (e.g., mesh motion, gas sensible heating, pore-space expansion, molecular weight). This definition simplifies the Cantera reactor network and allows for direct comparisons across model types (e.g., Type 1, Type 2, and our finite-rate chemistry model).

The temperatures are imposed by the solid-phase ablator temperature, implemented as the isothermal temperature of each CSTR. Pyrolysis rates are imposed by the Arrhenius decomposition models in the Aria simulation and implemented as CSTR inlets, as previously mentioned. From this bulk mass production rate, species production was derived from a simple speciation model; namely: a  $\beta$ -lookup table of species mole fractions measured by Bessire and Minton at 6.1°C/s (Fig. 4) [10]. In addition, gas species flow from the previous reactor in the network, via a separate inlet reservoir. Effective velocities are obtained from the Darcy-flow solver in Aria, and the current element lengths are found via the resulting deformed element dimensions from the Aria solution. This velocity along with the width of each element in Aria determines the residence time for each reactor, which is enforced by the initial set reactor mass. The reactor volume is not a state variable and is instead allowed to vary to maintain a constant pressure. Steady-state conditions are enforced on the bulk gas flow ( $\dot{m}_{in} = \dot{m}_{out}$ ) but not chemistry (reactor simulations proceed for a

set discretized time, rather than until a chemical steady state is reached). As previously discussed, secondary pyrolysis reactions are modeled using the kinetic database of Blanquart [13].

The general simulation setup is as follows: The CSTR network is originally initialized at t=0 of the Aria simulation results. Reactor inlet mass flow, temperature, and residence time are set based on the collected relevant results (effectively an inert ablator at this stage). The initial gas composition is set to pyrolysis gases generated at 300 K, per the results of Bessire and Minton. After initialization, the reactor network is advanced in time 0.05 seconds, matching the fixed timestep from the Aria simulation. At that point, the reactors are reinitialized using the data from the next timestep, with the gas composition in each reactor maintained from the prior network. The process is then repeated for the full time of the Aria simulation. The result is an examination of the evolution of the pyrolysis gas over time as the TACOT ablator is consumed during re-entry, allowing for the examination of transient flux in gas chemistry and heat transfer.

The energy balance of the isothermal CSTR is similar to that presented previously for ablation calculations, but chemical non-equilibrium increases the complexity. Namely, the Aria thermal simulations rely on the legacy assumptions that collapse pyrolysis-gas state variables to a single temperature-dependent state function. However, under finite-rate chemistry, three relevant chemical states exist for each reactor, namely those of (1) the gases entering from the prior PSR in the network  $(h_{g,i})$ , (2) the gases "generated" within the reactor via resin decomposition  $(h_{g,\omega})$ , which enter the reactor via a secondary inlet, and (3) the gases exiting the PSR, following all chemical reactions  $(h_{g,o})$ .

With this considered, the pyrolysis gas-pick-up and decomposition terms are calculated via:

$$\dot{q}_{decom} = h_{decom} \dot{\omega}_g = (h_{g,\omega} - \bar{h}) \dot{\omega}_g \tag{20}$$

$$\dot{q}_{pgpu} = -\frac{\partial h_g}{\partial x} \overline{m}_g'' = \left( h_{g,o} - h_{g,\omega} \right) \dot{\omega}_g + \frac{h_{g,o} - h_{g,i}}{\Delta x} m_{g,i}''$$
(21)

where  $\dot{\omega}_g$ ,  $\Delta x$ , and  $\dot{m}_{g,i}^{"}$  are computed from the Aria solution data.

Decomposition heating quantifies the heat of the resin-decomposition reaction based on the decomposition rate and the enthalpy of the decomposition reaction. The definition of  $\dot{q}_{pgpu}$  includes sensible and chemical enthalpies (i.e., sensible heating of gases and any chemical reactions thereof). Under the assumption of near-immediate chemical equilibrium (e.g. the primary pyrolysis gases  $h_{g,\omega}$  are assumed to be at chemical equilibrium before being added to the reactor), enthalpy changes due to rapid secondary pyrolysis reactions are accounted for in Eq. (20). Under the finite-rate Cantera study, any enthalpy changes to the pyrolysis gases generated within the element  $(h_{g,\omega})$  caused by gas-phase secondary pyrolysis are instead captured in  $\dot{q}_{pgpu}$ . This conceptual difference (e.g., gases generated in non-equilibrium vs equilibrium states) will become apparent in thermal analysis results in Sec. IVC.

Three metrics were devised to examine chemical activity in the Cantera simulation. The first is normalized gas enthalpy, which compares the gas enthalpy in its present state and to its "frozen" and "equilibrium" states:

$$\hat{h} = \frac{|h_g - h_{frzn}|}{|h_{equil} - h_{frzn}|} \tag{22}$$

The equilibrium gas mixture is simply acquired by taking the gas composition inside the reactor and bringing it to equilibrium under constant temperature and pressure, using Cantera's built-in functionality [17]. The frozen gas enthalpy refers to the expected composition of the gas with no active chemical kinetics. This composition is typically realized at low temperatures where chemical kinetics are stymied. This mixture is acquired by repeating the full Cantera simulation with chemical reactions disabled and measuring the enthalpy of the resulting composition at each timestep and location in the original simulation. A normalized enthalpy of 0 indicates that the gas is chemically frozen, while a value of 1 represents the gas reaching chemical equilibrium. A value in-between indicates an active non-equilibrium chemical state, described as the "active" chemical regime herein. This metric is imperfect for describing chemistry but directly evaluates the impact to simulation enthalpies.

Two further quantities of interest evaluate the chemical state. Reaction and advection rates are compared using the Damköhler number, calculated as:

$$Da = \frac{\text{Rate of Reaction}}{\text{Rate of Advection}} = \frac{\tau_R \sum_{i=0}^{n} r_i^+}{\rho}$$
 (23)

where  $\tau_R$  is the reactor residence time,  $r_i^+$  is the creation rate of species i, and  $\rho$  is the overall mixture mass density. At a very large Damköhler number (Da >> 1), chemistry approaches an infinite rate relative to advection, typically allowing the equilibrium-chemistry assumption. At a very small Damköhler number (Da << 1), chemistry is very slow relative to advection, typically allowing the frozen-chemistry assumption. At intermediate Damköhler numbers (Da  $\sim$  1), chemical and advection rates are comparable, typically requiring finite-rate chemistry to fully resolve.

For pyrolyzing ablators, analysis of the Damköhler number is informative for determining the relevance of chemical kinetics under the applied environmental conditions. However, the standard Damköhler number cannot resolve the exact transition between active and equilibrium chemistry regimes. For this reason, a second form of the Damköhler number, Da\*, is considered for net species generation. As this metric also incorporates species consumption, the metric should be relatively small at chemical equilibrium, allowing for better visualization of the transition from active to equilibrium chemical state. The modified Damköhler number is:

$$Da^* = \frac{\tau_R \sum_{i=0}^n (r_i^+ - r_i^-)}{\rho}$$
 (24)

### IV. Results

# A. Aria Results and Overall Gas Properties

Results from the Aria simulation of Case 1 and Case 2 are shown in Fig. 8. Ablator temperature, gas velocity, mass flow rate, and reaction extent are plotted as a function of distance from the surface. The observed in-depth heating, pyrolysis, and recession behavior appear nominal to the benchmark results of Lachuad [15]. As the ablator surface undergoes aeroheating, heat penetrates the ablator and decomposition occurs, the formed pyrolysis gas advects toward the surface. As the phenolic nearest the surface fully decomposes ( $\beta \sim 1$ ), a char region forms and the pyrolysis zone advances deeper into the ablator. Meanwhile, surface recession due to oxidation is modeled via the TACOT B' table and is modeled via a uniform mesh displacement of the Aria elements. In the early stages, the applied aeroheating leads to rapid heating and decomposition of the surface elements, increasing mass flow rate and delaying thermal penetration. Over time, a quasi-steady pyrolysis front forms in the ablator, with relatively consistent in-depth gas phase conditions. This effect is due to the near-constant applied aeroheating ( $q_{aero}^{"}$ ) flux at the surface, approximately 550 W/cm<sup>2</sup> for Case 1 and 36 W/cm<sup>2</sup> for Case 2. A significant material recession occurs in both cases; the observed recession was found to be almost perfectly linear, with a final ablator length at t = 120.1 seconds of 21.64 mm and 25.98 mm for Case 1 and 2 respectively. Pressure variation in-depth was negligible, with all cells maintaining close to atmospheric pressure throughout the simulation. Notably, the low-heating rate case reaches much lower temperatures, which will later impact the chemical kinetics results.

The Aria results drive the Cantera simulations. Figure 9 shows preliminary holistic results from Cantera, namely pyrolysis-gas enthalpy and average molecular weight for both test cases versus reactor (or ablator element) temperature. Cantera simulations were executed at every timestep of the Aria simulations; the solid lines in Fig. 9 represent the mean values across time for both cases. The shaded regions bound the maximum and minimum observed values across the full dynamic simulation for the respective cases. TACOT values are also included for initial comparison. The predicted enthalpies and molecular weights generally differ from TACOT, but molecular weights agree at low and high temperatures.

Despite dynamic evolution of the ablator, predicted gas properties do not vary significantly at equivalent temperatures over time or between the two cases. The higher variations in enthalpy and weight in the low-temperature regime can be explained by the primary pyrolysis model, which is governed by reaction extent,  $\beta$ , rather than temperature directly. At moderate temperatures (~1200-1800 K), the gas properties become consistent as primary pyrolysis ceases and the gas enters the char zone. These consistent properties are perhaps attributable to a consistent mixture of pyrolysis species in the char zone, arising from full decomposition of a thermally thick ablator. Namely, once the pyrolysis front is established, the gases entering the char zone include speciation at all reaction extents. Moreover, the gas-phase chemistry in the pyrolysis zone should be sufficiently frozen to maintain a consistent species composition. The increased uncertainty at higher temperatures, as seen in Case 1, is likely due to the onset of homogeneous gas-phase chemistry. However, the overall variation across time remains relatively small due to the formation of a quasi-steady pyrolysis and char zones in the ablator, which result in similar residence times and environmental conditions for the pyrolysis gas across all phases of the simulation. Of course, the existence of these quasi-steady conditions may primarily stem from the Ablation Test Cases used in this work, and quantified uncertainty of these properties may vary under more realistic re-entry conditions.

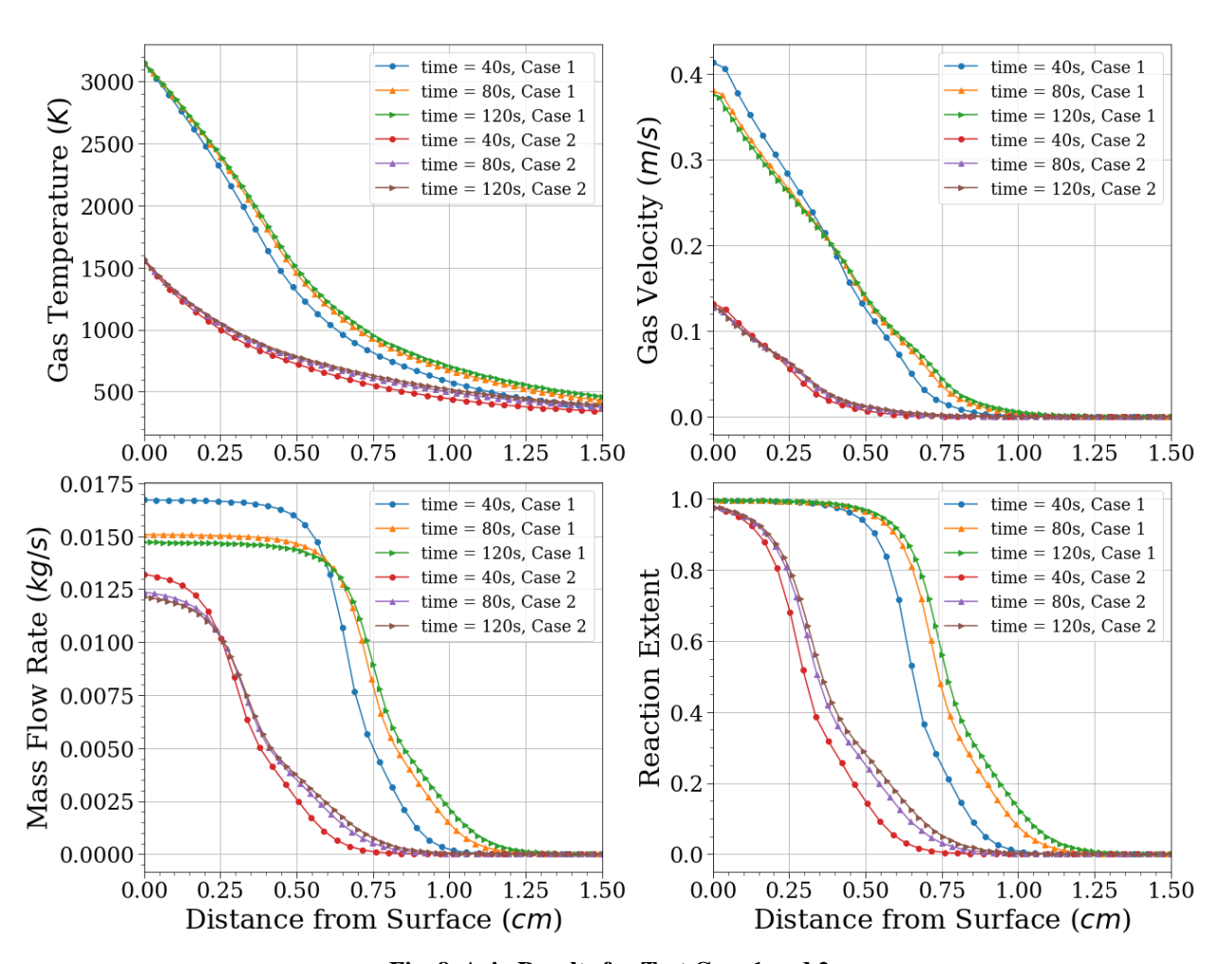


Fig. 8 Aria Results for Test Case 1 and 2

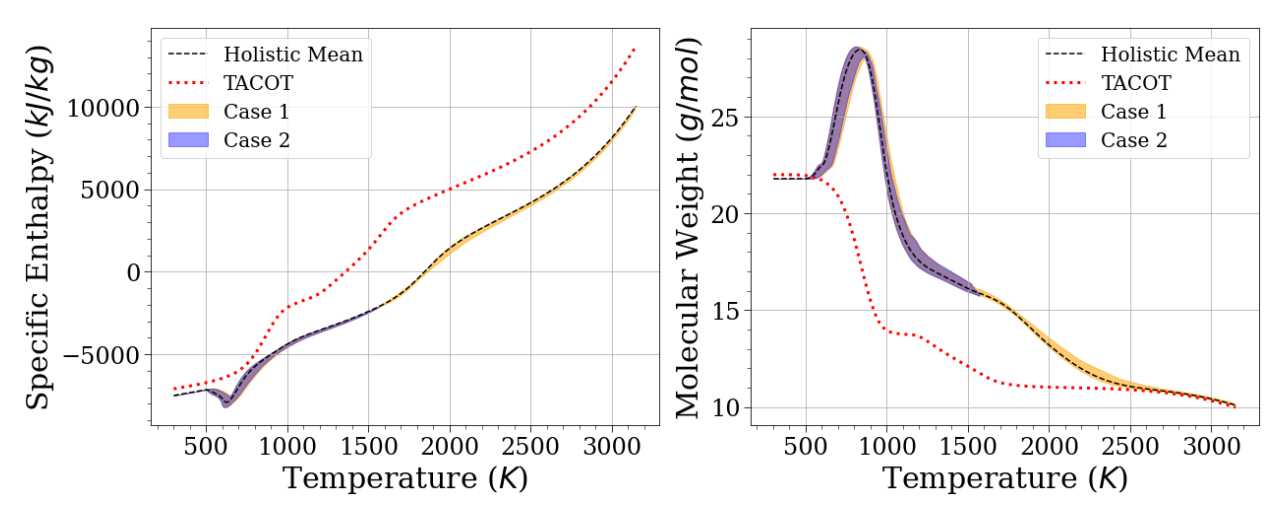


Fig. 9 Observed Variation of Pyrolysis Gas Properties over Total Simulation Time

## B. Finite Rate Kinetics and Gas Enthalpy

A more thorough analysis of the pyrolysis gases is provided by isolating Cases 1 and 2 at t = 120 seconds. This down selection was justified for several reasons. The results in Fig. 8 suggest that the variance in pyrolysis-gas chemistry between cases and across time therein is not extreme. Instead, a standing front propagates through the

material over time. By analyzing a timestep late in the ablation, this standing front is better discretized by the Cantera domain.

The influence of the non-uniform speciation model on elemental mass fractions of pyrolysis gases is displayed in Fig. 10. The elemental concentrations vary significantly below 1000 K, corresponding to peak decomposition rates. As the gas enters regions of near-fully charred ablator, the elemental composition stabilizes. For both cases, the composition of the pyrolysis gas converges to the expected average composition derived from the Bessire and Minton data in Fig. 3. As will be demonstrated, elemental variation predominantly occurs only while chemistry is frozen (e.g., T<1375 K).

The bulk enthalpy of the simulated pyrolysis gases is shown in Fig. 11. We compare here the enthalpy of the finite-rate Cantera CSTR network results to estimated frozen and equilibrated gas compositions, as well as TACOT. The  $\hat{h}$  metric indicates the transition between chemistry regimes (frozen, active, equilibrium). At low temperatures, the chemical kinetics are slow, and the pyrolysis gas is effectively in a frozen state. After about 1375 K, finite-rate-model enthalpy increases significantly relative to the frozen state, as the gas enters the active regime. As denoted by  $\hat{h}$ , the active-gas enthalpy remains in an intermediate state between frozen and equilibrium until about 2500 K, where enthalpy converges with equilibrium results. The gas of the low heating rate Case 2 remains far from chemical equilibrium (<1600 K) upon exiting the ablator and corresponds closely with the frozen state.

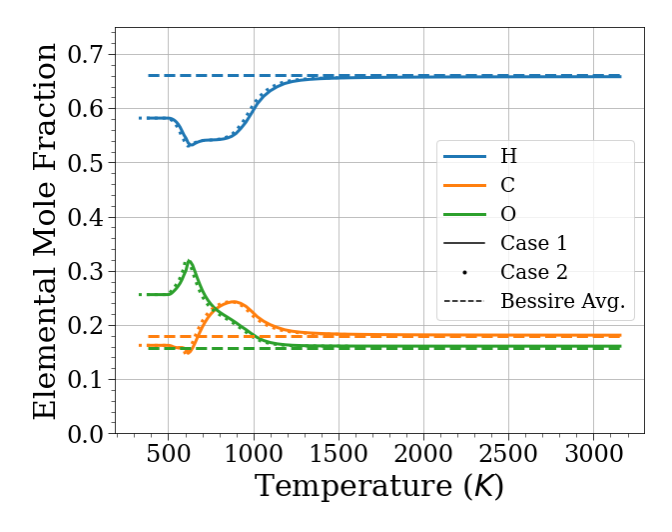


Fig. 10 Pyrolysis Gas Elemental Mass Fractions, t = 120 seconds

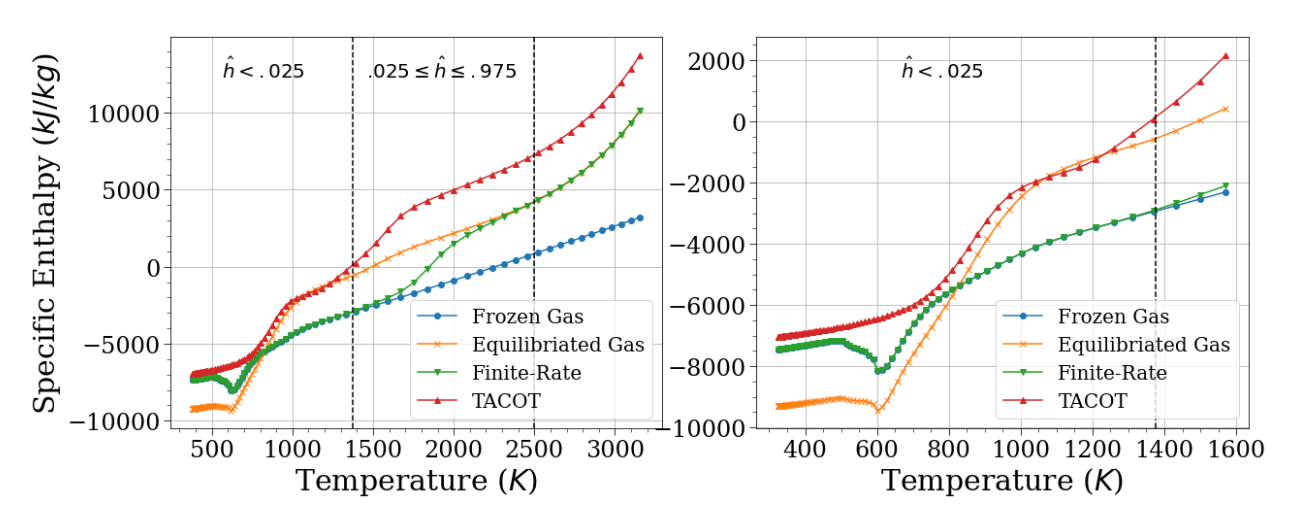


Fig. 11 Pyrolysis Gas Enthalpy Values for Case 1 (Left) and Case 2 (Right), t = 120 seconds

Figure 12 presents the standard and modified Damköhler numbers and further explores the chemical kinetics. As expected, the modified Damköhler number better segregates the different chemical regimes, particularly for Case 1.

Da\* begins to rise at ~1200 K, experiences several local peaks in activity between 1500 and 2300 K, then falls to near-zero above 2700 K, ostensibly as the gas approaches equilibrium. The shape of the curve suggests a roughly three-step reaction process, with peaks of chemical reactivity observed at approximately 1500, 1900, and 2200 K. In Case 1 a slight increase in Da\* occurs near the surface, likely due to alterations in the equilibrium composition with temperature. The behavior for Case 2 shows near-identical behavior, though the pyrolysis gas only experiences the first peak in chemical reactivity before exiting the ablator surface.

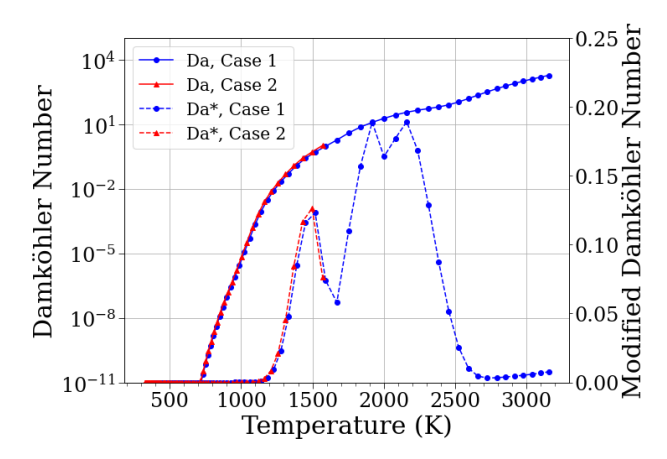


Fig. 12 Damköhler Numbers, t = 120 seconds

Examination of the individual gas species further reveals the chemical processes underway. Figure 13 shows the mass fraction of major species over the observed gas temperature range for Case 1, compared to the expected equilibrium composition based on the species in the Blanquart mechanism [13]. Prominent non-equilibrium species and processes are evident. Moving from lower- to higher-temperature, initial species concentrations fluctuate at low temperatures (<1200 K), due to primary pyrolysis. A comparison between both plots in Fig. 13 shows that primary pyrolysis gases are relatively far from chemical equilibrium. A breakdown of larger primary pyrolysis products, such as Phenol, Toluene, and Cresol, occurs at 1500K and corresponds to the first Da\* peak seen in Fig. 12. Thereafter, intermediate products form including benzene (C<sub>6</sub>H<sub>6</sub>) and noticeable concentrations of PAH products (A<sub>1</sub>C<sub>2</sub>H, A<sub>2</sub>-C<sub>10</sub>H<sub>8</sub>, A<sub>2</sub>R<sub>5</sub>, etc.). The amount of PAH products peaks at around 5% of the mixture mass fraction, significantly lower than predicted by Rabinovitch [12]. This discrepancy is likely due to the higher elemental fraction of oxygen in the present study. PAH is disfavored at higher temperatures and begins to break down along with benzene at around 1900 K, corresponding to the second Da\* peak. In the final reaction peak, the breakdown of H<sub>2</sub>O, CH<sub>4</sub>, and CO<sub>2</sub> occurs, completing fully around 2500 K, and the gas mixture converges with the expected equilibrium state. A separate analysis of Case 2 results (not shown) revealed nearly identical behavior over its modeled temperature range.

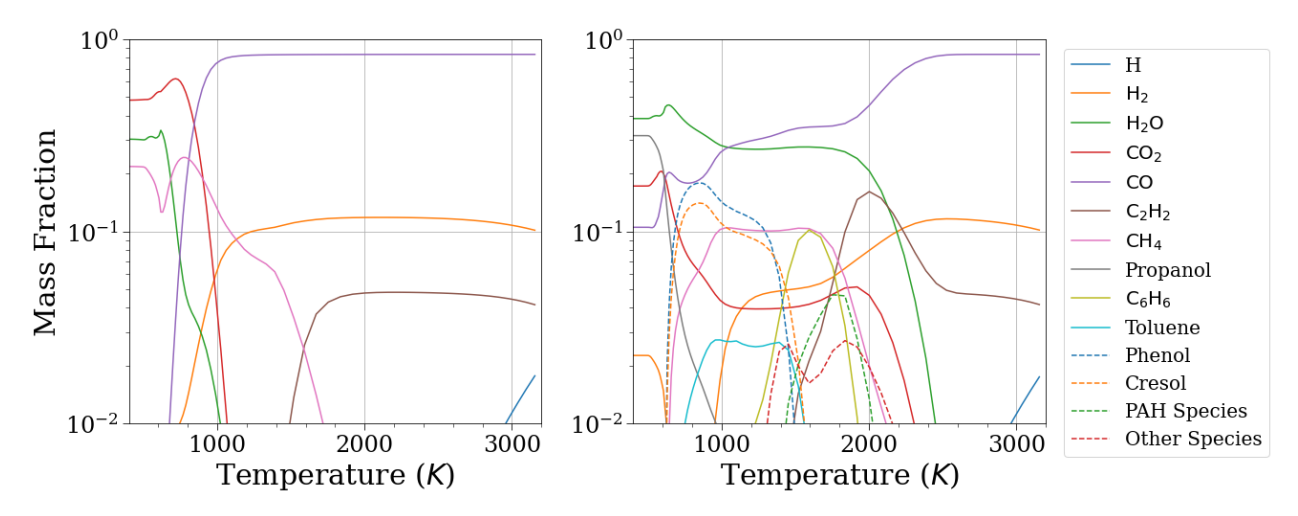


Fig. 13 Pyrolysis Gas Species Composition at Equilibrium (Left) vs. Finite-Rate Results (Right), t = 120 seconds, Case 1

## C. Thermal Transport

Utilizing the calculated Cantera gas properties, volumetric heat absorption from both transpiration cooling and phenolic decomposition was resolved spatially. Focusing first on decomposition, Fig. 14 shows the computed heat of reaction ( $h_{decom}$ ) for the various gas compositions of Case 1. Notably, this term appears to be negative for all mixtures below 900 K. As the majority of pyrolysis gas is usually generated below this temperature, this implies a net exothermic primary pyrolysis process. These exothermic reaction enthalpies are likely a result of the leveraged TACOT material properties [15]. The provided thermal material properties (conductivity, specific heat, etc.) are for the full composite material. The virgin and charred formation enthalpies of the TACOT composite (-857.1 kJ/kg and zero respectively) assume a formation enthalpy of zero for both the phenolic char and carbon fiber matrix. The former assumption appears to differ with experimental results, which report a non-zero, temperature-dependent formation enthalpy for SC-1008 char as well as a lower virgin resin value (-2440 kJ/kg vs the -2000 kJ/kg value used for TACOT) [27]. Additionally, the virgin and char-specific heat values used from the TACOT database to compute enthalpies in Eq. (14) were calibrated by matching FIAT model predictions with experimental arc jet data [28]. The authors of the original study warn that the data should not be considered independent of FIAT, and its use in alternative codes may result in inaccurate performance predictions. In short, the thermochemical properties of TACOT are not necessarily accurate enough to expect agreement of reaction enthalpies to empirical results.

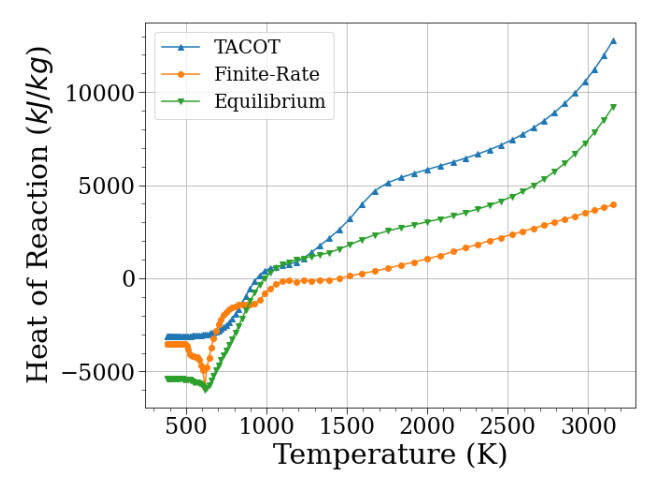


Fig. 14 Heat of Decomposition ( $h_{decom}$ ) for Case 1, t = 120 seconds

Figure 15 shows the spatially derived results for  $\dot{q}_{aecom}$  and  $\dot{q}_{pgpu}$  for both cases at 120 seconds. As expected from the previous figure, both the finite-rate and equilibrium speciation models yield a net exothermic decomposition, for both Case 1 and 2. For each result, two distinct peaks form in the ablator, roughly aligned with peak decomposition rates from the 2-reaction mechanism of Goldstein in Table 1. Both TACOT and the Cantera-computed equilibrium gas enthalpy predict a strongly exothermic (negative) decomposition reaction, with a shift to endothermic behavior at higher temperatures coinciding with the second decomposition peak. For the finite-rate results, both peaks remain exothermic.

The transpiration cooling  $\dot{q}_{pgpu}$  is directly calculated from the gas enthalpy results in Fig. 11. As a result, the equilibrium and finite-rate cooling converges near the surface for the high-temperature Case 1. Further in-depth, the equilibrium gas produces two peaks in heat absorption, resulting from significant shifts in the computed equilibrium composition and enthalpy, as seen in Fig. 13. Unsurprisingly, TACOT exhibits similar behavior, though with a significantly more endothermic the second peak. In contrast, the finite-rate results show a large single peak, encompassing cells where the gas is in the active chemical regime. The size of the second peak for finite-rate gas compensates for the first peak, ultimately attaining similar net heat absorption. Importantly, the Case 2 finite-rate results lack this region of enhanced cooling, as the gas exits the ablator in a near-frozen state.

Figure 16 shows the evolution of the overall thermal effect of these terms over time by integrating over the ablator length, yielding overall energy flux q'' at each timestep. This term can be considered analogous to the ablator surface energy balance terms discussed in Sec. II, and directly compares the impact of transpiration and decomposition to surface heating, such as the applied aerothermal surface flux. As seen previously in Fig. 15, both the finite-rate and equilibrium models show an exothermic decomposition over most simulation times of very similar magnitude. An exception is at earlier simulation timesteps, where the equilibrium  $q_{decom}^{''}$  becomes strongly endothermic, while the

finite-rate results diverge and become more exothermic. The observed transient divergence arises from rapid heating near the surface at the onset of the simulation, biasing decomposition to higher temperatures where equilibrium models are more endothermic. Presuming TACOT thermo-physical properties are representative of real ablators, this general trend suggests that decomposition during low-heating rate cases and experiments may generally be more exothermic than those at faster rates.

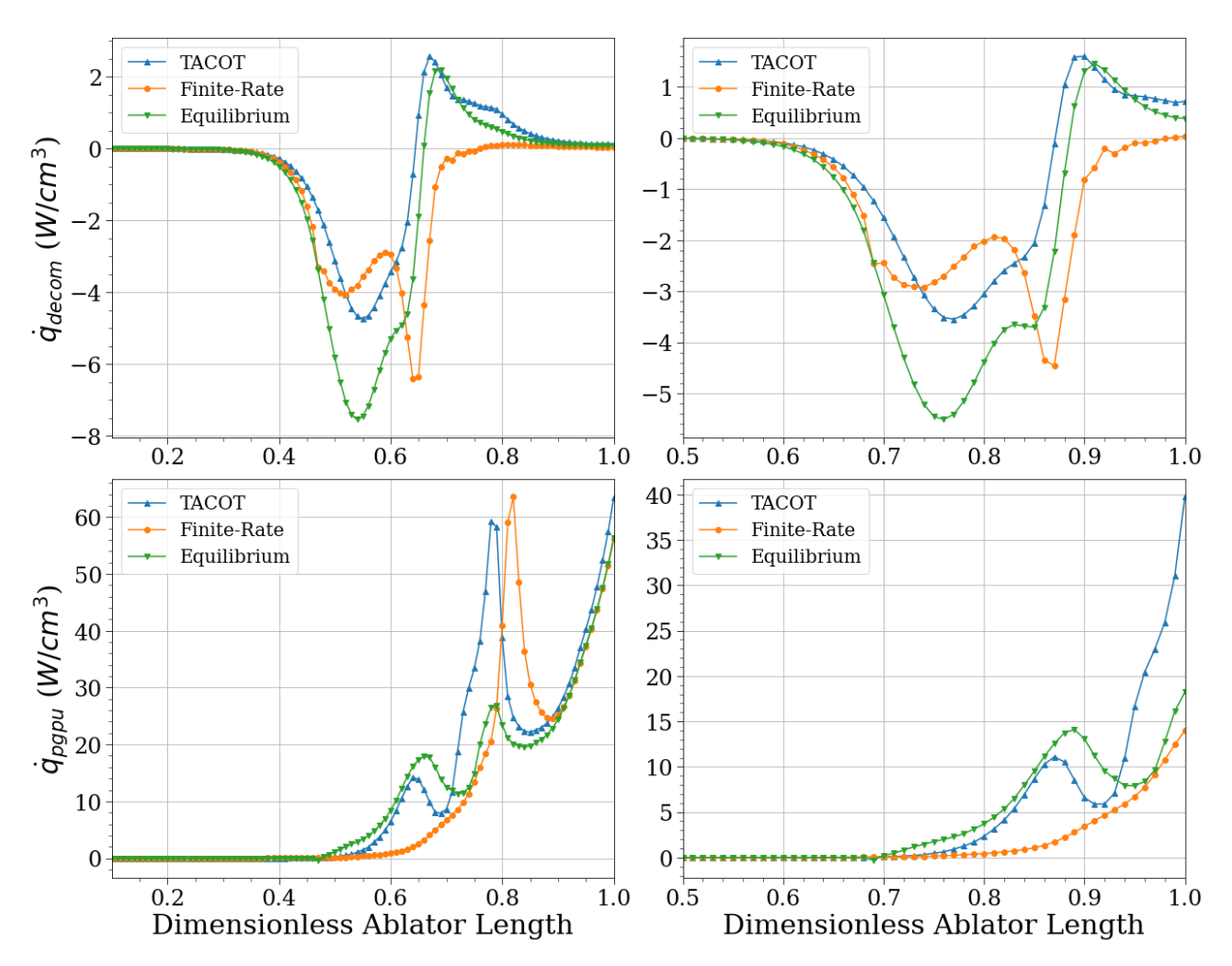


Fig. 15 Pyrolysis Gas Thermal Response for Case 1 (Left) and Case 2 (Right), t = 120 seconds

Total transpiration energy flux  $(q_{pgpu}^{"})$  values for both cases show a similar dichotomy between the spatial and transient results, though the impact of utilizing the legacy assumption is much more apparent. The results of the previous section revealed that in-depth chemical equilibrium requires higher temperatures that are only obtained in Case 1. If, as in Case 1, equilibrium conditions are attained before the ablator surface, the overall predicted heat absorption is near-identical between the finite-rate and equilibrium assumptions, though the spatial distribution is still impacted significantly, as seen in Fig. 15. In Case 2, equilibrium is not obtained in the finite-rate model and total heat absorption is reduced by over 50% relative to the equilibrium model. Compared to the applied aerothermal surface flux for Case 2 (~ 36 W/cm²), we see that the computed  $q_{pgpu}^{"}$  is not insignificant in comparison, suggesting a potentially significant impact on the overall ablator energy balance.

In summary, if sufficiently high temperatures (>2500 K) are not reached, the traditional assumption of pyrolysis gas chemical equilibrium appears invalid and could significantly alter the overall energy balance. Utilization of the equilibrium assumption may also mischaracterize the spatial distribution of thermal effects in-depth, impacting comparisons to thermocouple readings and substrate temperatures. In fact, the equilibrium generally *overpredicts* gasrelated cooling effects on the ablator, thereby underpredicting thermal penetration. This observation is consistent with previous Type-3 modeling efforts, where the implementation of finite-rate chemistry leads to significantly higher indepth ablator temperatures [14]. These observations suggest that the incorporation of finite-rate chemistry into

material response codes may significantly impact ablation solutions, and future work in this area is highly recommended.

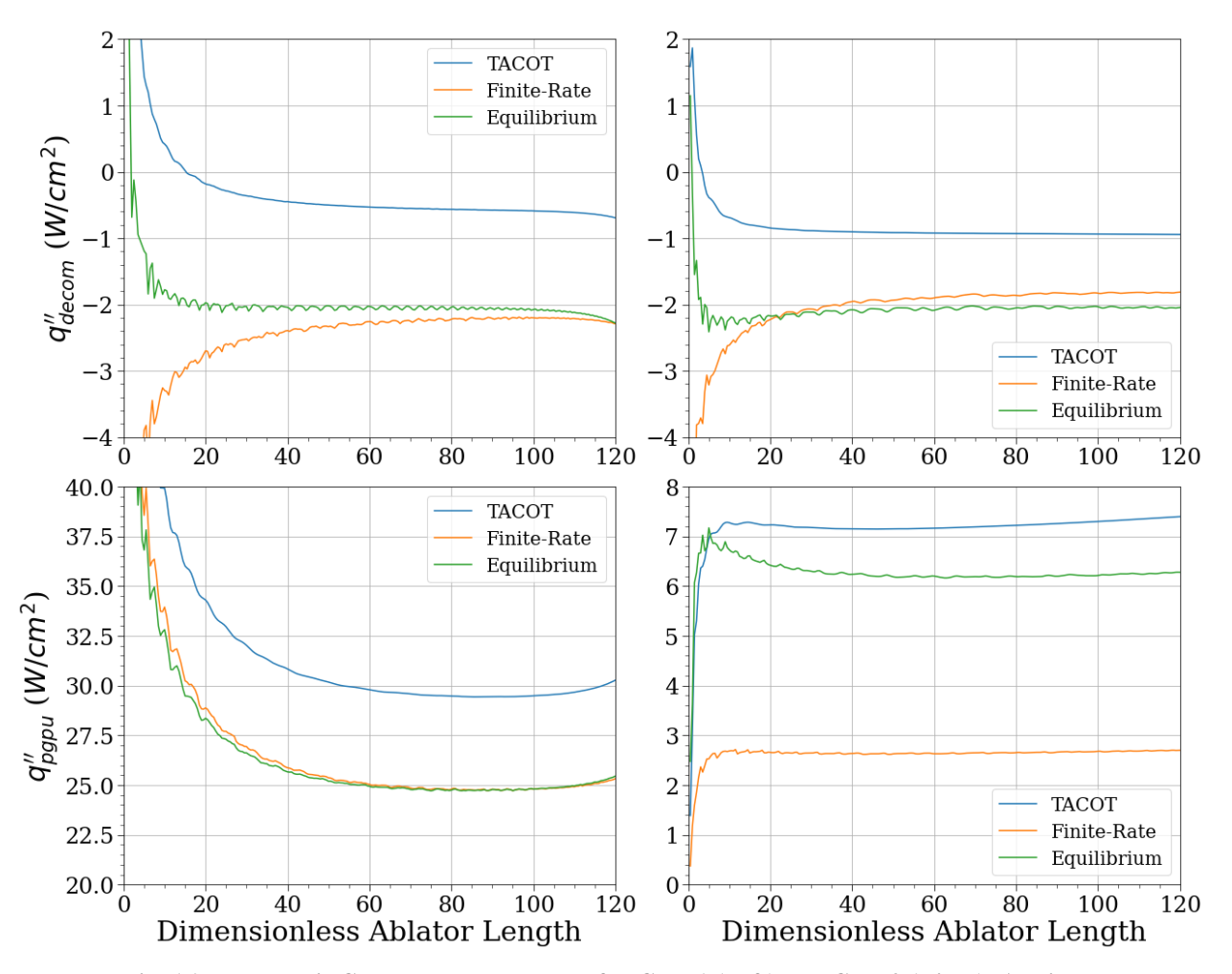


Fig. 16 Pyrolysis Gas Thermal Response for Case 1 (Left) and Case 2 (Right), All times

# V. Conclusion

This study sought to challenge the assumptions of equilibrium chemistry and constant elemental mass fractions for pyrolysis gases in ablation codes from a heat transfer perspective. A one-way coupling scheme was devised between Sandia National Laboratories' ablation capabilities in SIERRA/Aria and Cantera. The 2<sup>nd</sup> Ablation Test-Case Series was slightly modified and applied to 1D simulations of TACOT. These ablator-response predictions were then applied to Cantera, where a network of 0D continuously-stirred tank reactors simulated pyrolysis-gas chemistry. Utilizing recent experimental results of PICA pyrolysis and a robust chemistry model, the evolution of pyrolysis gas and related thermal effects were determined over a wide temperature range.

Primary pyrolysis of the phenolic resin was seen to generally occur in the low-temperature regime, with the elemental composition of the generated pyrolysis gas stabilizing around 1200 K. The simulations revealed that this gas experiences three distinct chemical regimes in the ablator. Below 1400 K, the pyrolysis gas is generally chemically inert compared to the advection timescale. Between 1400 and 2500 K, a region of active chemistry is observed, characterized by rapid changes in species composition. PAH formation in the gas mixture is noticeable in this temperature range, but at its peak constitutes a minor percentage of species mass and mole fractions before dissociating at higher temperatures. Above 2500 K, gases converge toward a near-equilibrium state.

The observed chemical kinetics have significant implications for the ablator thermal response, particularly for transpiration cooling. For the low heating rate case with a surface temperature of ~1500 K, the finite-rate model resulted in an overall predicted heat absorption over 50% lower than that predicted by equilibrated pyrolysis gas or

tabulated results of TACOT. Due to a convergence of gas enthalpy and species composition at higher temperatures, overall and near-surface ablator heat absorption between the two approaches converged for the high-heating rate case with a surface temperature approaching 3200 K. However, significant deviation is still observed in-depth.

Overall, these observed results suggest that the assumptions of equilibrium chemistry and constant elemental mass fractions for pyrolysis gases in ablation codes should be re-evaluated, and a more comprehensive understanding of pyrolysis gas chemistry is required for accurate predictions of ablator performance. Further simulations and modeling will be conducted to explore potential gas-surface effects and develop a more accurate uncertainty analysis of computed pyrolysis gas composition and enthalpy results.

# **Funding Sources**

This work was supported by the Laboratory Directed Research and Development program at Sandia National Laboratories, a multi-mission laboratory managed and operated by National Technology and Engineering Solutions of Sandia LLC, a wholly-owned subsidiary of Honeywell International Inc. for the U.S. Department of Energy's National Nuclear Security Administration under contract DE-NA0003525. Additional support was provided by a NASA Space Technology Graduate Research Opportunity (NSTGRO) Fellowship under grant 80NSSC21K1279.

# Acknowledgments

We appreciate the assistance of John Hewson and Andrew Kurzawski on early versions of the Cantera and Aria models.

#### References

- [1] Trick, K. A., and Saliba, T. E., "Mechanisms of the pyrolysis of phenolic resin in a carbon/phenolic composite," *Carbon*, vol. 33, 1995, pp. 1509–1515. https://doi.org/10.1016/0008-6223(95)00092-r
- [2] Ferguson, J. C., Panerai, F., Lachaud, J., and Mansour, N. N., "Theoretical study on the micro-scale oxidation of resin-infused carbon ablators," *Carbon*, vol. 121, 2017, pp. 552–562. https://doi.org/10.1016/j.carbon.2017.06.013
- [3] "User's Manual Aerothermal Charring Material Thermal Response and Ablation Program," Vol. 1,. Acurex Corporation, Mountain View, California, AFPRL-TR-70-92, April 1970.
- [4] Chen, Y.-K., and Milos, F. S., "Ablation and thermal response program for spacecraft heatshield analysis," *Journal of Spacecraft and Rockets*, vol. 36, 1999, pp. 475–483. https://doi.org/10.2514/2.3469
- [5] Lachaud, J., Magin, T., Cozmuta, I., and Mansour, N. N., "A Short Review of Ablative Material Response Models and Simulation Tools," 7th Aerothermodynamics Symposium, European Space Agency, Noordwijk, The Netherlands, May 2011, pp. 1–8.
- [6] Lachaud, J., van Eekelen, T., Scoggins, J. B., Magin, T. E., and Mansour, N. N., "Detailed chemical equilibrium model for porous ablative materials," *International Journal of Heat and Mass Transfer*, vol. 90, 2015, pp. 1034–1045. <a href="https://doi.org/10.1016/j.ijheatmasstransfer.2015.05.106">https://doi.org/10.1016/j.ijheatmasstransfer.2015.05.106</a>
- [7] Wong, H.-W., Peck, J., Assif, J., Lachaud, J., and Mansour, N. N., "Quantitative determination of species production from the pyrolysis of the phenolic impregnated carbon ablator (PICA)," 53rd AIAA Aerospace Sciences Meeting, 2015. https://doi.org/10.2514/6.2015-1447
- [8] Wong, H.-W., Peck, J., Assif, J., Panerai, F., Lachaud, J., and Mansour, N. N., "Detailed analysis of species production from the pyrolysis of the phenolic impregnated carbon ablator," *Journal of Analytical and Applied Pyrolysis*, vol. 122, 2016, pp. 258–267.
- <a href="https://doi.org/10.1016/j.jaap.2016.09.016">https://doi.org/10.1016/j.jaap.2016.09.016</a>
   [9] Bennett, A., Payne, D. R., and Court, R. W., "Pyrolytic and elemental analysis of decomposition products from a phenolic resin," *Macromolecular Symposia*, vol. 339, 2014, pp. 38–47. <a href="https://doi.org/10.1002/masy.201300136">https://doi.org/10.1002/masy.201300136</a>
- [10] Bessire, B. K., and Minton, T. K., "Decomposition of phenolic impregnated carbon ablator (PICA) as a function of temperature and heating rate," ACS Applied Materials & Interfaces, vol. 9, 2017, pp. 21422–21437. https://doi.org/10.1021/acsami.7b03919
- [11] Sykes, G. F., "Decomposition Characteristics of a Char-Forming Phenolic Polymer Used for Ablative Composites," NASA TN, Vol. D3810, 1967, pp. 1–20.
- [12] Rabinovitch, J., Marx, V. M., and Blanquart, G., "Pyrolysis gas composition for a phenolic impregnated carbon ablator heatshield," 11th AIAA/ASME Joint Thermophysics and Heat Transfer Conference, 2014. https://doi.org/10.2514/6.2014-2246
- [13] Blanquart, G., Pepiot-Desjardins, P., and Pitsch, H., "Chemical Mechanism for High Temperature Combustion Engine Relevent Fuels with Emphasis on Soot Precursors," *Combustion and Flame*, Vol. 156, No. 3, 2009, pp. 588–607.

- https://doi.org/10.1016/j.combustflame.2008.12.007
- [14] Lachaud, J., and Mansour, N. N., "Porous-material analysis toolbox based on openfoam and applications," *Journal of Thermophysics and Heat Transfer*, vol. 28, 2014, pp. 191–202. https://doi.org/10.2514/1.t4262
- [15] J. Lachaud, A. Martin, T. van Eekelen, I. Cozmuta, Ablation test-case series #2, version 2.8, January 2011, 8 p.,5th Ablation Workshop, Feb. 28-March. 1, Lexington, Kentucky.
- [16] "Sierra Multimechanics module: Aria User Manual Version 4.56.," Sandia National Lab., SAND-2020-4000, Albuquerque, NM, April 2020.
- [17] Goodwin, D. G., Speth, R. L., Moffat, H. K., and Weber, B. W., "Cantera: An Object-oriented Software Toolkit for Chemical Kinetics, Thermodynamics, and Transport Processes," <a href="https://www.cantera.org">https://www.cantera.org</a>, 2021. Version 2.5.1.
- [18] Goldstein, H.W., "Pyrolysis Kinetics of Nylon 6-6, Phenolic Resin, and Their Composites," *Journal of Macromolecular Science*, Part A, Vol. 3, No. 4, 1969, pp. 649–673. https://doi.org/10.1080/10601326908053834
- [19] Torres-Herrador, F., Meurisse, J. B. E., Panerai, F., Blondeau, J., Lachaud, J., Bessire, B. K., Magin, T. E., and Mansour, N. N., "A high heating rate pyrolysis model for the phenolic impregnated carbon ablator (PICA) based on mass spectroscopy experiments," *Journal of Analytical and Applied Pyrolysis*, vol. 141, 2019, p. 104625. https://doi.org/10.1016/j.jaap.2019.05.014
- [20] Torres-Herrador, F., Coheur, J., Panerai, F., Magin, T. E., Arnst, M., Mansour, N. N., and Blondeau, J., "Competitive kinetic model for the pyrolysis of the phenolic impregnated carbon ablator," *Aerospace Science and Technology*, vol. 100, 2020, p. 105784.
  - https://doi.org/10.1016/j.ast.2020.105784
- [21] Oliver, B., "3D Material Response Analysis of PICA Pyrolysis Experiments," 9th Ablation Workshop, 2017.
- [22] Lachaud, J., Cozmuta, I., and Mansour, N. N., "Multiscale approach to ablation modeling of phenolic impregnated carbon ablators," *Journal of Spacecraft and Rockets*, Vol. 47, No. 6, 2010, pp. 910–921. <a href="https://doi.org/10.2514/1.42681">https://doi.org/10.2514/1.42681</a>
- [23] Hüttinger, K. J., "CVD in hot wall reactors—the interaction between homogeneous gas-phase and heterogeneous surface reactions," *Chemical Vapor Deposition*, vol. 04, 1998, pp. 151–158. https://doi.org/10.1002/(sici)1521-3862(199807)04:04<151::aid-cvde151>3.0.co:2-2
- [24] Driver, D., and MacLean, M., "Improved predictions of Pica recession in ARC jet shear tests," 49th AIAA Aerospace Sciences Meeting, 2011. https://doi.org/10.2514/6.2011-141
- [25] Freno, B. A., Carnes, B. R., Brunini, V. E., and Matula, N. R., "Nonintrusive manufactured solutions for non-decomposing ablation in two dimensions," *Journal of Computational Physics*, vol. 463, 2022, p. 111237. https://doi.org/10.1016/j.jcp.2022.111237
- [26] Collins, L., and Roberts, S. A., "Mesoscale simulation of woven composite design decisions," arXiv: Computational Engineering, Finance, and Science, Cornell University, 2021 (unpublished). <a href="https://doi.org/10.48550/ARXIV.2104.13554">https://doi.org/10.48550/ARXIV.2104.13554</a>
- [27] Ladacki, M., Hamilton, J. V., and Conz, S., "Heat of pyrolysis of resin in silica-phenolic ablator.," AIAA Journal, vol. 4, 1966, pp. 1798–1802. https://doi.org/10.2514/3.3780
- [28] Covington, M. A., Heinemann, J. M., Goldstein, H. E., Chen, Y.-K., Terrazas-Salinas, I., Balboni, J. A., Olejniczak, J., and Martinez, E. R., "Performance of a low density ablative heat shield material," *Journal of Spacecraft and Rockets*, vol. 45, 2008, pp. 237–247.
  - https://doi.org/10.2514/1.12403